Electrochemistry
The Electrochemical Society of Japan
Received: December 12, 2023
Accepted: March 16, 2024
Published online: March 22, 2024
Issued: to be determined.
https://doi.org/10.5796/electrochemistry.23-00142
https://doi.org/10.50892/data.electrochemistry.25448005
Article
Electrochemistry, (in press) 1–7

The Effect of Supply Rate of Li Ion and Anion on Li Dissolution/Deposition Behavior in $LiNO_3$ Electrolyte Solutions for Li-Air Batteries

Fumisato OZAWA,[a,*,§] Kazuki KOYAMA,[a] Daiki IWASAKI,[a,§] Shota AZUMA,[a,§] Akihiro NOMURA,[b,§] and Morihiro SAITO[a,*,§]

[a] *Faculty of Science and Technology, Seikei University, 3-3-1 Kichijoji-Kitamachi, Musashino, Tokyo 180-8633, Japan*
[b] *Center for Green Research on Energy and Environmental Materials, National Institute for Materials Science (NIMS), 1-1 Namiki, Tsukuba, Ibaraki 305-044, Japan*

* *Corresponding authors: fumisato-ozawa@st.seikei.ac.jp (F. O.), mosaito@st.seikei.ac.jp (M. S.)*

ABSTRACT

Although Li-air batteries (LAB) have a high theoretical energy density (3500 Wh kg^{-1}), further developments are required to overcome their practical limitations. Regarding the Li-metal negative electrode (NE), we have previously reported on the reversibility of the Li dissolution/deposition reaction by using Li|Li symmetric cells with a tetraglyme (G4)-based electrolytic solution. Particularly, in the 1.0 M (= mol L^{-1}) $LiNO_3$/G4 electrolyte under an O_2 atmosphere, a Li_2O protective layer is efficiently formed on the Li-metal electrode at a current density of 0.40 mA cm^{-2}, and Li dendrite formation is suppressed. In the present study, we expanded the test conditions (current densities up to 2.0 mA cm^{-2} and temperatures of 10 to 50 °C) to clarify the dissolution/deposition behavior of the Li-metal NE. The effects of two electrolyte solutions, namely LiTFSI/G4 and $LiNO_3$/G4, on the Li-metal NE were evaluated based on cyclical testing using Li|Li symmetric cells under an O_2 atmosphere. The NEs were also examined by scanning electron microscopy and X-ray photoelectron spectroscopy. The results indicated that not only $LiNO_3$ salt but also the supply of Li and nitrate ions at the Li electrode surface are critical factors in LAB performance.

Keywords : Li Metal Anode, Li Dissolution/deposition, $LiNO_3$ Electrolyte Solution, Li-air Battery (LAB)

1. Introduction

Lithium-air batteries (LAB) have attracted much attention because of their theoretical energy density, reaching as high as 3500 Wh kg^{-1}.[1] However, all the components of LAB cells, specifically the air electrodes (positive electrode, PE), lithium electrodes (negative electrode, NE), and electrolyte solutions, have some drawbacks and must be developed further. In addition to its role as the active material in PEs, oxygen dissolves into the electrolyte solution and diffuses to the NE to react with the surface of Li-metal in LABs employing nonaqueous electrolyte solutions, forming a passivation film composed of Li_2O.[2–4] We previously studied the effect of oxygen on the lithium NE (Li NE) in three tetraglyme (G4)-based electrolyte solutions with different electrolyte salts: lithium trifluoromethanesulfonate ($LiSO_3CF_3$; LiOTf), lithium bis(trifluoromethylsulfonyl) imide ($LiN(SO_2CF_3)_2$; LiTFSI), and lithium bis(fluorosulfonyl) imide ($LiN(SO_2F)_2$; LiFSI).[5] The Li|Li symmetric cells with different electrolyte solutions performed differently under an argon or oxygen atmosphere. Notably, the Li deposition/dissolution reaction was improved by the introduction of O_2 for all electrolytes.

Lithium nitrate ($LiNO_3$) is considered a useful Li salt for stabilizing the interface between organic electrolyte solutions and Li-metal electrodes,[6–8] and it has been applied to stabilize the Li NE surface in LABs.[9–12] $LiNO_3$ not only reacts and forms an oxide film on the surface of Li-metal NE but also works as a redox mediator. The bifunctional effect of O_2 and $LiNO_3$ on the surface of the Li metal has recently been reported.[13,14] A 1.0 M (= mol L^{-1}) $LiNO_3$/N,N-dimethylacetamide electrolyte solution was used, and the results suggested that the coexistence of O_2 and $LiNO_3$ ensured stable cyclability while reducing the change in impedance. Recently, we reported that $LiNO_3$ in a G4-based electrolyte solution showed high cycle performance under an O_2 atmosphere, compared with LiOTf and LiTFSI.[15] These differences are attributed to the chemical interactions between the Li-metal electrode and the anions, namely OTf^-, $TFSI^-$, and NO_3^-, in the G4 solvent and oxygen atmosphere, producing dissolved oxygen and its active intermediate products. However, it was not determined how $LiNO_3$ in a G4-based electrolyte solution affected the Li NE in practical applications, assuming rapid charge/discharge and low or high temperatures. The factors that affect the supply of Li^+ to the Li electrode surface, such as the Li^+ ion concentration, solvent viscosity, degree of dissociation, and ionic conductivity in the electrolyte, are important to investigate for efficient Li dissolution and deposition.

Herein, we applied wider test conditions (current densities from 0.20 to 2.0 mA cm^{-2} and temperatures of 10 to 50 °C) to clarify the dissolution/deposition behavior of the Li electrode. We compared the effects of two lithium salts, LiTFSI and $LiNO_3$, on Li NE performance in G4-based electrolyte solutions by performing discharge/charge cycle tests using Li|Li symmetric cells under controlled current densities and temperatures. We also conducted scanning electron microscopy energy-dispersive X-ray spectroscopy (SEM-EDS) and X-ray photoelectron spectroscopy (XPS) analyses of the deposits on the NE.

2. Materials and Methods

2.1 Preparation of electrolytes

$LiNO_3$ (Sigma-Aldrich, ≥99.99 %) were dried in a vacuum oven at 110 °C overnight before dissolution. LiTFSI (Kishida Chemical, ≥99.9 %) and dried $LiNO_3$ were handled in an Ar-filled glove box

§ECSJ Active Member
F. Ozawa orcid.org/0009-0008-7214-0885

(Miwa, MDB-1BK-NT1). Each Li salts were dissolved in tetraethylene glycol dimethyl ether (G4, Nippon Nyukazai, <10 ppm H_2O) at the concentration of 1.0 M. The H_2O contents of the electrolyte solutions were quantified to be under 100 ppm using a Karl Fisher titration apparatus (CA-31, Mitsubishi Chemical Analytech). The ionic conductivity, viscosity, and density of each electrolyte solution at 25–60 °C were ascertained using a pH/ion meter (SevenExcellence S500, Mettler Toledo) and a rolling-ball viscometer (Lovis2000ME, Anton Paar), respectively.

2.2 Electrochemical measurements

Li|Li symmetric cells were assembled using Li metal foil (thickness: 0.5 mm, Honjo Metal) as both electrodes, a separator (Celgard 2400, Celgard), and each electrolyte in an argon filled glove box. The Li|Li symmetric cells were used for Li dissolution/deposition cycle tests under an O_2 atmosphere at 10, 30, and 50 °C. The O_2 atmosphere was prepared by purging Ar out of the assembled cells using high-purity O_2 gas (G1 grade, >99.99995 %) injected at 200 mL min^{-1} for 15 s. The applied current density was 0.20 to 2.0 mA cm^{-2} at a maximum dissolution/deposition capacity of 0.50 mAh cm^{-2} in the voltage range between −2.0 and 2.0 V for 15 cycles.

2.3 Electrode analysis

After 15 cycles, the Li-metal electrodes were picked out the Li|Li symmetric cells and rinsed with fresh G4 solvent to remove the Li salts in an Ar-filled glove box. After drying under vacuum, the electrodes were placed in a transfer vessel to avoid exposure to air. The morphology and composition of the deposited films were evaluated by SEM-EDS (JSM-7800F, JEOL). Cross-section samples of Li-metal electrodes were treated using an Ar ion beam in a JEOL cross polisher IB-09020CP at an accelerating voltage of 8 kV for 3 h at 0 °C.

In addition, the chemical bonding state and elemental composition of the Li electrode surface after Li dissolution/deposition were examined by XPS (ULVAC PHI, VersaProbe II). After 15 cycles, the Li-metal electrode was rinsed with G4, dried sufficiently, placed in a transfer vessel, and transported to the main chamber for analysis, without exposure to the atmosphere. In the XPS measurements, the acceleration voltage and emission current of a monochromatic AlKα X-ray (1484.6 eV) were set at 15 kV and 3 mA, respectively. Peak fits and baseline correction of all spectra were performed using Origin Pro Peak Analyzer. The binding energy scale was calibrated using the hydrocarbon C 1s peak at 285.0 eV.

3. Results and Discussion

3.1 Cycle tests at 0.50 mAh cm^{-2}

Figure 1 shows dissolution/deposition cycle test results for the cells using 1.0 M LiTFSI/G4 electrolyte solutions. The graphs exhibited relatively low overvoltages, which suggests a stable surface state of the Li electrode. At a lower current density (0.20 mA cm^{-2}), the voltage decreased up to the 15th cycle, which was likely caused by the sufficient stability of the surface film, and the continuous gradual decrease of the voltage thereafter is ascribed to the increased effective surface area caused by dendrite deposition (Fig. 1A). In contrast, at a higher current density (0.40 to 2.0 mA cm^{-2}), the voltage significantly changed from the first cycle, and unstable polarization curves were obtained (Figs. 1B–1E). These results suggested that the Li_2O layer protecting the Li-metal electrode protection from O_2 could not withstand the current density and the exposed Li metal reacted with the solvent and anion, resulting in the growth of Li dendrites. Moreover, the overvoltage decreased when the operating temperature was raised to 10, 30, and 50 °C, suggesting that the diffusion rate of Li^+ ions in the electrolyte was improved and the charge transfer resistance during the reaction was reduced (Figs. S1A–S1C). The correlation was also suggested from the physical properties of the electrolyte, as the Li^+ diffusion coefficient and Li ion transference number increased as the temperature rose (Table S1). At 10 and 30 °C, the flatness of the polarization curve collapsed from the first cycle (Figs. S1A–S1B), implying that the solvent decomposed. In addition, the overvoltage gradually decreased, suggesting the formation of Li dendrites during the dissolution and deposition cycle, which increases the specific surface area of the Li electrode. The flat part of the polarization curve was depressed even at 50 °C, indicating that Li dendrites formed in the LiTFSI/G4 electrolyte under all operating temperatures (Fig. S1C). The potential fluctuation was suppressed by raising the operating temperature, suggesting that electrolyte decomposition was suppressed.

Figure 2 shows that cells with the 1.0 M $LiNO_3$/G4 electrolyte solution exhibited larger overpotentials after the first cycle, mainly because this electrolyte has the lowest ionic conductivity, 0.22 mS cm^{-1}. The overvoltage gradually increased with additional

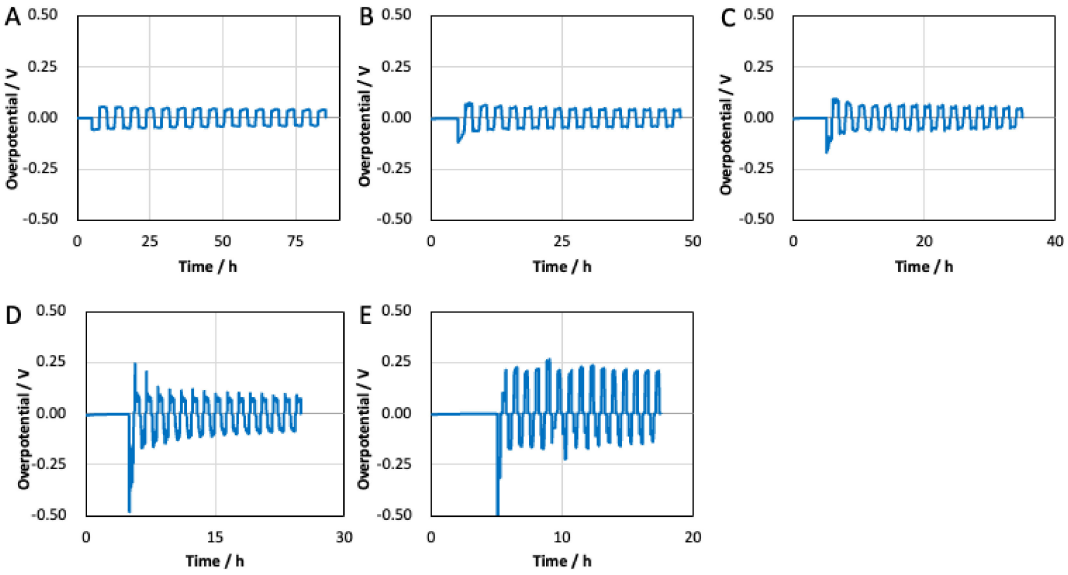

Figure 1. Polarization curves of the Li|Li symmetric cells tested at 0.40 mAh cm^{-2} and 30 °C using the LiTFSI electrolyte and different current densities: (A) 0.20, (B) 0.40, (C) 0.60, (D) 1.0, and (E) 2.0 mA cm^{-2}.

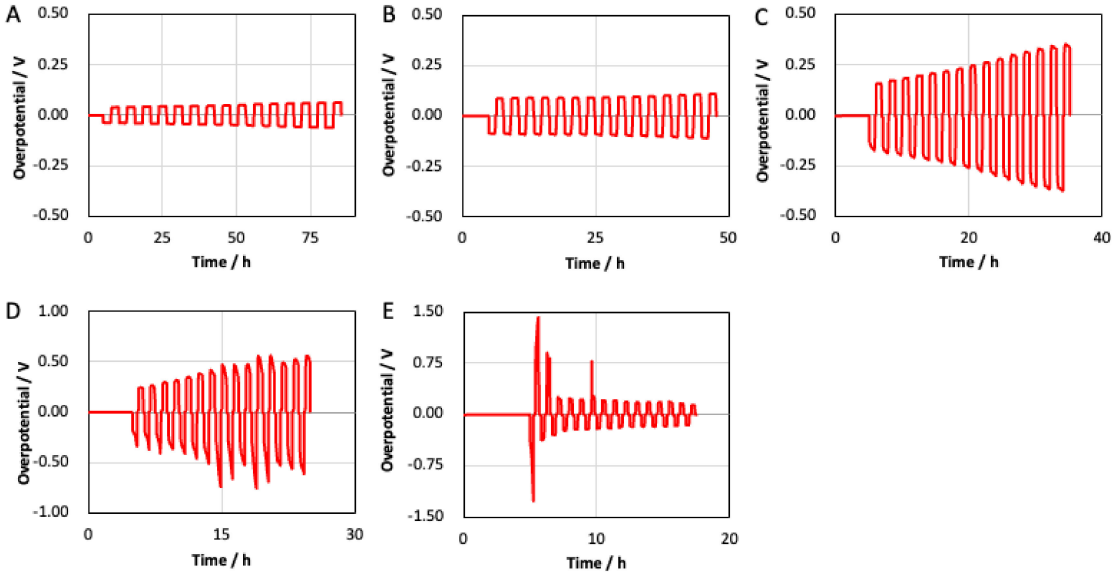

Figure 2. Polarization curves of the Li|Li symmetric cells tested at 0.40 mAh cm^{-2} and 30 °C using the $LiNO_3$ electrolyte and different current densities: (A) 0.20, (B) 0.40, (C) 0.60, (D) 1.0, and (E) 2.0 mA cm^{-2}.

cycles, suggesting an accumulation of Li deposited on the surface (Fig. 2A). The flat polarization curves indicate that no dendritic growth occurred.[16] However, the overvoltage also increased for 0.4 and 0.6 mA cm^{-2} (Figs. 2B–2C). Above 1.0 mA cm^{-2}, the flatness of the polarization curve was lost, suggesting that electrolyte decomposition occurred (Figs. 2D–2E). Moreover, the overvoltage decreased for increasing operating temperatures, similar to LiTFSI/G4, suggesting that the diffusion rate of Li^+ ions in the electrolyte was improved and the charge transfer resistance during the reaction was reduced (Figs. S2A–S2C). In fact, although $LiNO_3$/G4 electrolyte had a lower ionic conductivity than LiTFSI/G4, but had the diffusion coefficient of Li^+ equal to or higher than that of LiTFSI/G4 (Table S1). This is owing to the solvation structure of Li^+ in the electrolyte solutions. In the case of LiTFSI salt electrolyte, relatively large amount of Li^+ was dissociated form $TFSI^-$ anion compared with $LiNO_3$ salt one and the Li^+ solvated by G4 solvent diffused. Therefore, the diffusion radius was relatively large. On the other hand, $LiNO_3$ salt was poorly dissociated in the G4-based electrolyte and the contact ion pairs of Li^+-NO_3^- diffused with a rather small diffusion radius. Conversely, at the low temperature of 10 °C, the flatness of the polarization curve was poor, and the overvoltage gradually decreased (Fig. S2A). This also suggests that Li dendrites formed, increasing the specific surface area of the Li electrode during dissolution and deposition. Nevertheless, the overvoltage was not reduced to the extent observed for the LiTFSI electrolyte, indicating that solvent decomposition was not observed. Thus, the $LiNO_3$/G4 electrolyte affects solvent decomposition even at 10 °C. At 30 and 50 °C, the flatness of the polarization curve was maintained, and the change in the overvoltage with additional cycles was small (Figs. S2B–S2C). Therefore, the diffusion rate of Li ions increased at higher operating temperatures, and Li ions diffused to the electrode surface more quickly, suppressing the formation of Li dendrites. Since the diffusion coefficient of solvent and Li^+ increase as the temperature increases, it is assumed that the diffusion of nitrate anions also increased. Even if the Li_2O protective layer was partially broken and the Li-metal electrode was exposed during Li dissolution and deposition, the electrode immediately reacted with nitrate anions to form a solid-electrolyte interphase (SEI) film. The SEI formation can reduce the uneven spots and suppress Li dendrite formation.

The differences in performance between cells using LiTFSI and $LiNO_3$ electrolytes demonstrated the effect of the Li_2O protective layer formed on the Li NE surface by the reaction between the Li metal and NO_3^-.

3.2 Surface analysis of the electrode after 15 cycles at 0.50 mAh cm^{-2}

Figure 3 shows SEM images of the Li NE surfaces after 15 cycles in the 1.0 M LiTFSI/G4 and 1.0 M $LiNO_3$/G4 electrolyte solutions. A larger dendrite surface area was observed for LiTFSI/G4 (Figs. 3A–3C) than for $LiNO_3$/G4 (Figs. 3D–3E). At 0.20 mA cm^{-2} in LiTFSI/G4, flat deposits covered the whole surface, and Li dendrites were observed (Fig. 3A). A similar morphology was observed for 0.60 to 2.0 mA cm^{-2}, but with areas of exposed Li metal, indicating that the deposits were fragile (Figs. 3B–3C). As the current density increased, the decomposition of the electrolyte progressed, resulting in the deposition of fine Li dendrites and decomposition products.[17] These results are also consistent with the Li dissolution/deposition results shown in Fig. 1, which suggests the continuous deposition of dendrites and decomposition products. In addition, the Li dendrites become thicker at higher operating temperatures (Figs. S1D–S1F). Because the deposits easily peeled off, the anion and solvent were likely decomposed. A different morphology was observed for Li NEs in $LiNO_3$/G4 (Figs. 3D–3F), revealing dense deposition without dendrite formation, even above 0.40 mA cm^{-2}. As the current density increased, numerous granular depositions were observed, which consist of electrolyte decomposition products, such as Li_2CO_3, and agglomerated Li_2O particles that peeled off the surface.[18] Furthermore, the granular deposits were present on the electrode surface at 10 °C, suggesting that the diffusion rate of Li ions was slower than the rate of Li dissolution and deposition, and the electrolyte decomposed (Fig. S2D). In contrast, at 30 and 50 °C, Li dendrites and granular deposits did not form on the electrode surface (Figs. S2E and S2F). In $LiNO_3$, no easy-to-exfoliate deposits or no Li dendrites were observed. The $LiNO_3$/G4 electrolyte effectively suppressed Li dendrite growth even at 10 °C and suppressed electrolyte decomposition to some extent.

Figure 4 shows cross-sectional SEM images of Li NEs after 15 cycles at 0.40 mA cm^{-2} in the 1.0 M LiTFSI/G4 and 1.0 M $LiNO_3$/G4 electrolyte solutions. Approximately 30 µm-thick sediments and locally 70 µm-thick pit-shaped sediments were observed for LiTFSI/G4 (Figs. 4A–4B), suggesting that Li dissolution/deposition progressed locally owing to the formation of a non-uniform SEI

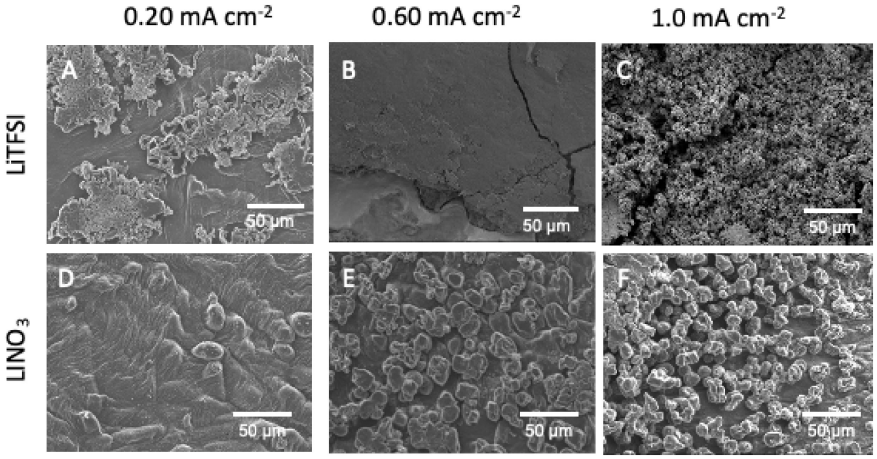

Figure 3. SEM images of Li NE surfaces after 15 cycles at 0.20, 0.60, and 1.0 mA cm^{-2} in different electrolyte solutions: (A–C) LiTFSI/G4 and (D–F) $LiNO_3$/G4.

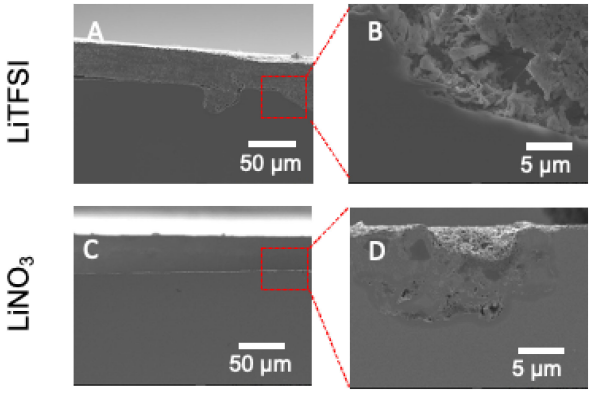

Figure 4. Cross-sectional SEM images of Li NEs after 15 cycles at 0.40 mA cm^{-2} in different electrolyte solutions: (A–B) LiTFSI/G4 and (C–D) $LiNO_3$/G4.

layer. In contrast, thin sediment was observed for $LiNO_3$/G4 (Figs. 4C–4D), suggesting that Li dissolution/deposition progressed uniformly owing to the formation of a uniform SEI layer.[19,20]

Figure 5 shows the SEM-EDS mapping of the O Kα and C Kα signals. Tables S2 and S3 summarize the results for the Li electrode surface after 15 cycles at different current densities in LiTFSI/G4 and $LiNO_3$/G4, respectively. In LiTFSI/G4, the sediment contains substantial amounts of F and S, and the elemental ratio F : S is distributed at 3 : 1. At the interface between the Li metal and the sediment, C and O accumulate on the Li-metal side, whereas it does not appear on the Li-metal surface, suggesting that the solvent decompose on the Li-metal surface (Figs. 5A–5C). However, the Li dendrite grows away from the Li-metal surface. These results suggested that Li dissolution and deposition at 0.40 mA cm^{-2} progressed without a uniform SEI layer and the Li electrode surface was not completely protected. On the other hands, the oxygen distribution was uniform in $LiNO_3$/G4, suggesting that the Li_2O layer is spread uniformly (Figs. 5D–5F). In addition, the mapping of C consistent with O, suggesting that Li_2CO_3 was also deposited. To compare of the LiTFSI, the ratio of oxygen was large, indicating that the ratio of Li_2CO_3 and solvent decomposition products was smaller.

Figure 6 shows the XPS spectra of Li NE surfaces after 15 cycles in 1.0 M LiTFSI/G4 at different current density. Analysis of the C 1s peak revealed solvent decomposition peaks such as C-O (286.9 eV) and C=O (287.7 eV). A peak for Li_2CO_3 (289.7 eV) was also found, which was consistent with the polarization curve and EDS mapping, showing that electrolyte decomposition occurred. This was consistent with the observation of peaks such as Li (54.5 eV) and Li_2CO_3 (55.4 eV) in Li1s spectra. Furthermore, we found that the Li_2O layer formed by O_2 remained even at 0.40 mA cm^{-2}. However, the suppression of Li dendrite growth could not be confirmed from the SEM image. From these results, Li dissolution and deposition at a high rate in a TFSI electrolyte solution does not have the effect of suppressing Li dendrite growth using the Li_2O layer formed by O_2 and the decomposition of the electrolyte solution. The samples operated at 0.40 and 0.60 mA cm^{-2} both exhibited C 1s peaks, which appeared to be C-F (291.6 eV), indicating the decomposition of electrolyte anions.

Figure S3 shows the XPS spectra of Li NE surfaces after 15 cycles at 10, 30, and 50 °C. The C 1s spectra at each temperature revealed signals of solvent decomposition, such as the peaks for C-O and C=O. The signal of Li_2CO_3 decreased as the temperature increased from 10 °C, showing that higher operating temperatures improved Li-ion diffusion and suppressed electrolyte decomposition. In addition, the suppression of Li dendrites could not be confirmed from SEM images, suggesting that the LiTFSI/G4 electrolyte did not suppress the growth of Li dendrites using the Li_2O layer formed by O_2.

Figure 7 shows the XPS spectra of Li NE surfaces after 15 cycles in 1.0 M $LiNO_3$/G4 at different current density. Considering that the peaks derived from Li_2CO_3 are strong in C 1s and Li 1s, electrolyte decomposition occurred, and many decomposition products were deposited on the Li NE surface. However, the flatness of the polarization curve suggests that electrolyte decomposition was not serious and the formation of Li_2CO_3 suppressed excessive electrolyte decomposition. In addition, the peaks derived from C=O and C-O were smaller than the peaks derived from Li_2CO_3, implying that solvent decomposition was suppressed. For the Li 1s spectra, no peak derived from Li_2O (55.7 eV) was observed at 0.2–0.6 mA cm^{-2}, indicating that Li_2O was not exposed on the top surface of the Li NE. In contrast, a peak of Li_2O appeared at 1.0 mA cm^{-2}, suggesting that Li_2O was partially exposed on the top surface of the Li NE. These results indicate that in the 1.0 M $LiNO_3$/G4 electrolyte, Li_2CO_3 covered the Li NE surface during Li dissolution and deposition, even at a high rate above 0.60 mA cm^{-2}. The Li NE in the 1.0 M $LiNO_3$/G4 electrolyte exhibited enhanced reversibility owing to the preferential reduction of $LiNO_3$ and the formation of an inorganic-rich SEI.[6,21,22] This observation can be attributed to the anions localized on the Li-metal surface, resulting from the reaction: $2Li + NO_3^- \rightarrow Li_2O + NO_2^-$ on the Li-metal

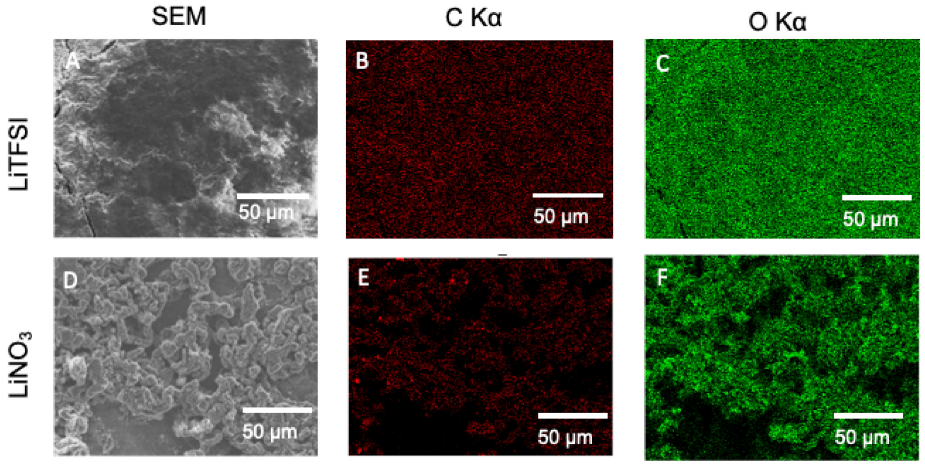

Figure 5. SEM-EDS compositional mapping of Li NE surfaces after 15 cycles at 0.40 mA cm^{-2} in different electrolyte solutions: (A–C) LiTFSI/G4 and (D–F) $LiNO_3$/G4.

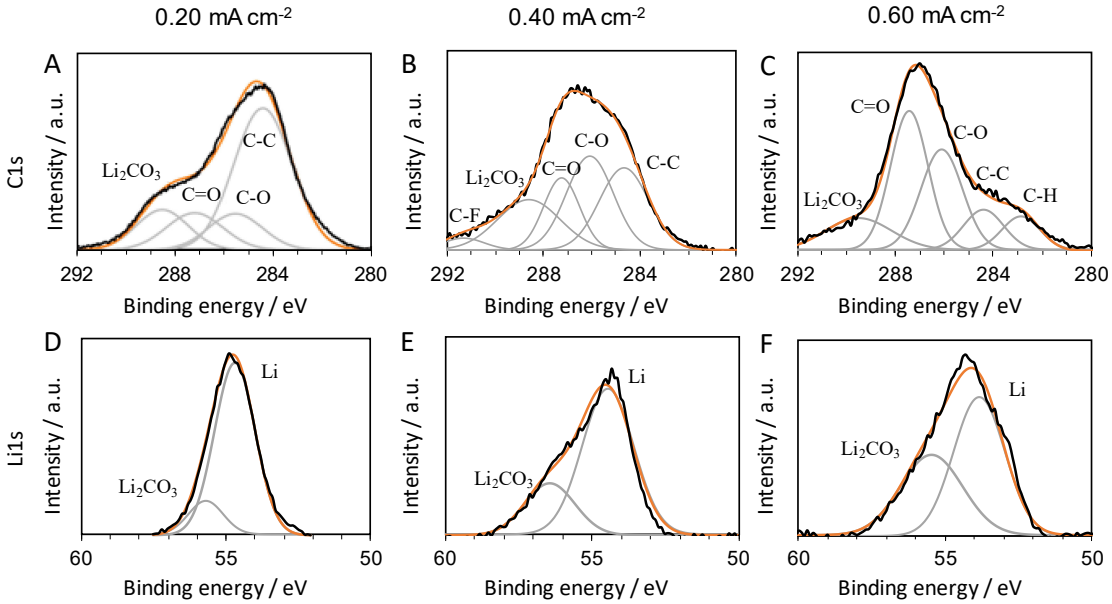

Figure 6. XPS spectra of the Li NE surface after 15 cycles in 1.0 M LiTFSI/G4. (A–C: C 1s and D–F: Li 1s)

surface. However, NO_2^- produced was smoothly oxidized back to NO_3^- by dissolved O_2, and it has almost no effect on the NO_3^- concentration localized on the Li NE surface.[23] These phenomena suppressed excessive electrolyte decomposition and Li dendrite growth.

Figure S4 shows the XPS spectra of Li NE surfaces after 15 cycles at 10, 30, and 50 °C. Analysis of the C 1s spectra at each temperature revealed signals of solvent decomposition, such as the peaks for C-O and C=O. In addition, a peak was observed for Li_2CO_3, consistent with the polarization curve, suggesting that electrolyte decomposition occurred. Moreover, Li_2O was not detected in the Li 1s spectra at 10 and 30 °C, indicating that Li_2O was not exposed on the top surface of the Li NE after 15 cycles. Figures S4D–S4F confirms that $LiNO_3$/G4 electrolyte suppressed Li dendrite growth and electrolyte decomposition using the Li_2O layer formed by O_2. These results indicate that electrolyte decomposition products, such as Li_2CO_3, were deposited on the Li_2O layer. The signal of Li_2O also appeared at 50 °C, suggesting that higher operating temperatures can suppress electrolyte decomposition.

3.3 Models of surface reactions and morphology depending on the supply of ions

Based on the results, we modeled the surface reactions and morphology on the Li NE, as shown in Fig. 8. Using 1.0 M $LiNO_3$/G4, the flatness of the polarization curve was maintained for operation below 0.60 mA cm^{-2}. The Li-ion diffusion was sufficient, and stable Li dissolution and deposition progressed. The oxygen derived from NO^{3-} in the electrolyte was highly active and efficiently produced inorganic SEI components such as Li_2O and Li_2CO_3. In contrast, the flatness of the polarization curve was lost above 1.0 mA cm^{-2} because the ion reaction rate was insufficient, resulting in electrolyte decomposition. Thus, the diffusion of ions in the electrolyte affected the Li dissolution and deposition behavior.

Regarding the Li dissolution/deposition behavior at high temperatures, the polarization curve shows that overvoltage was reduced, and the electrolyte decomposition was suppressed. This is due to improved Li-ion diffusion in the electrolyte, which allows Li ions to quickly reach the Li electrode surface before the electrons are used in other reactions. Furthermore, in the $LiNO_3$/G4 electrolyte, the diffusion of nitrate anions improved in addition to the diffusion

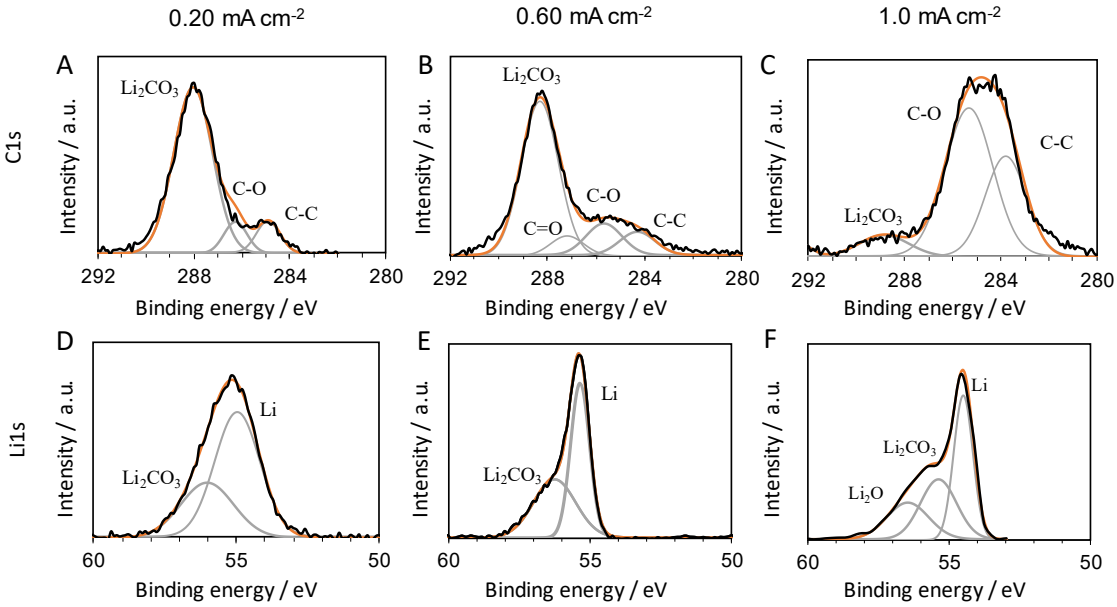

Figure 7. XPS spectra of the Li NE surface after 15 cycles in 1.0 M $LiNO_3$/G4. (A–C: C 1s and D–F: Li 1s)

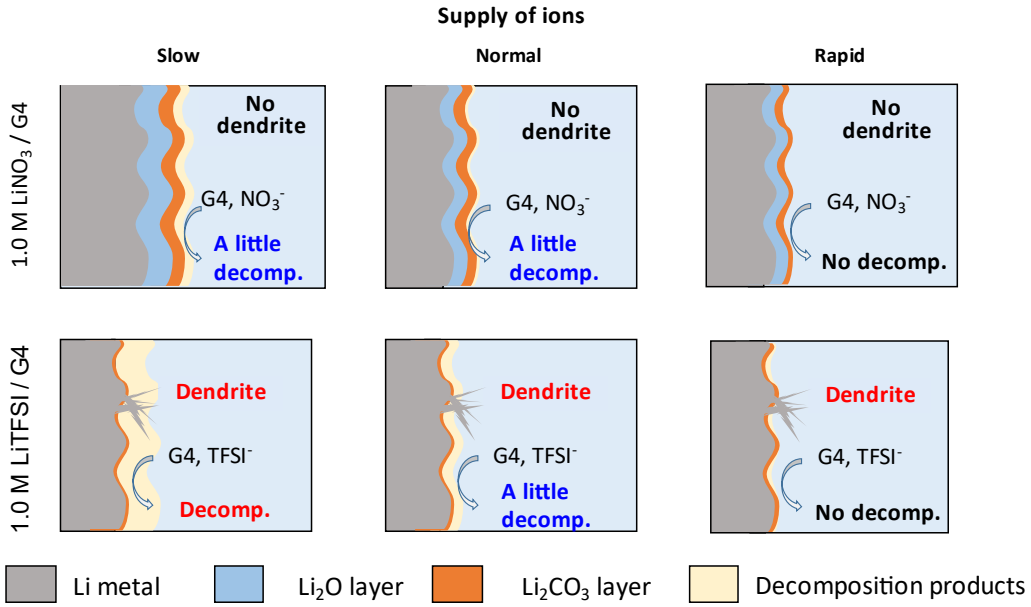

Figure 8. Models of the surface reactions and morphologies that occur depending on the supply of ions.

of Li ions, which allowed them to reach the Li electrode surface more smoothly, generating SEI films comprising Li_2O and Li_2CO_3. This reduced the exposure of the Li metal and promoted dissolution/deposition while suppressing side reactions. In addition, operating at high temperatures improved Li diffusion and suppressed the side reactions even at high current densities that require more Li.

However, the overvoltage increased when the diffusion of Li ions was suppressed at low temperatures. In the $LiNO_3$/G4 electrolyte, although the overvoltage increased compared with the test at 30 °C, the flatness of the polarization curve was maintained, indicating that the Li_2O protective layer suppressed Li dendrite growth. In contrast, solvent decomposition was observed at the beginning of the cycle tests in the LiTFSI/G4 electrolyte, and the electrode surface was covered with solvent decomposition products. The Li dissolution/deposition rate is faster than the formation rate of the Li_2O protective layer, resulting in solvent decomposition and non-uniform Li dissolution and deposition.

4. Conclusions

Two electrolyte solutions, LiTFSI/G4 and $LiNO_3$/G4, were compared regarding their effect on the Li NE during cycling Li|Li symmetric cells under an O_2 atmosphere. In addition to the cycling performance at different current densities and temperatures, the morphology and composition of the Li NE surface were examined by SEM and XPS. Using the LiTFSI/G4, the polarization curves were unstable and the NE surface was accompanied by Li dendrite growth. Whereas using the $LiNO_3$/G4, the polarization curves were stable and the NE surface did not exhibit Li dendrite formation. These differences were due to the chemical interactions between the Li-metal electrode and the anions, $TFSI^-$ and NO^{3-}, in the G4 solvent and O_2. Particularly, the O_2 derived from NO^{3-} in the $LiNO_3$/G4 electrolyte was highly active and produced inorganic SEI components such as Li_2O and Li_2CO_3. Cycle tests under controlled current densities and temperatures confirmed the stability of the Li-

metal electrode in the $LiNO_3$/G4 electrolyte solution. Our findings demonstrate that not only $LiNO_3$ salt but also the supply of Li and nitrate ions at the NE surface are critical factors in LAB performance. Additionally, it is necessary to quickly form protective films, such as Li_2O or Li_2CO_3, with appropriate thicknesses.

Acknowledgment

This work was partly supported by the Japan Science and Technology Project for the Next Generation Batteries Area in Advanced Low Carbon Technology Research and Development (ALCA-SPRING JPMJAL1301) and the National Institute for Materials Science (NIMS) Joint Research Hub Program. The SEM-EDS and XPS measurements were performed at the NIMS Battery Research Platform.

CRediT Authorship Contribution Statement

Fumisato Ozawa: Conceptualization (Equal), Project administration (Supporting), Writing – original draft (Lead)
Kazuki Koyama: Data curation (Lead), Formal analysis (Lead)
Daiki Iwasaki: Data curation (Supporting), Formal analysis (Supporting)
Shota Azuma: Formal analysis (Supporting), Methodology (Supporting)
Akihiro Nomura: Writing – review & editing (Supporting)
Morihiro Saito: Conceptualization (Equal), Project administration (Lead), Writing – review & editing (Lead)

Data Availability Statement

The data that support the findings of this study are openly available under the terms of the designated Creative Commons License in J-STAGE Data listed in D1 of References.

Conflict of Interest

The authors declare no conflict of interest in the manuscript.

Funding

Japan Science and Technology Agency: ALCA-SPRING JPMJAL1301
National Institute for Materials Science: NIMS Joint Research Hub Program

References

D1. F. Ozawa, K. Koyama, D. Iwasaki, S. Azuma, A. Nomura, and M. Saito, *J-STAGE Data*, https://doi.org/10.50892/data.electrochemistry.25448005, (2024).
1. P. G. Bruce, S. A. Freunberger, L. J. Hardwick, and J.-M. Tarascon, *Nat. Mater.*, **11**, 19 (2012).
2. D. Aurbach, Y. Gofer, and J. Langzam, *J. Electrochem. Soc.*, **136**, 3198 (1989).
3. D. Aurbach, M. Daroux, P. Faguy, and E. Yeager, *J. Electroanal. Chem. Interfacial Electrochem.*, **297**, 225 (1991).
4. D. Aurbach and O. Chusid, *J. Power Sources*, **68**, 463 (1997).
5. M. Saito, T. Fujinami, S. Yamada, T. Ishikawa, H. Otsuka, K. Ito, and Y. Kubo, *J. Electrochem. Soc.*, **164**, A2872 (2017).
6. C. Yan, Y.-X. Yao, X. Chen, X.-B. Cheng, X.-Q. Zhang, J.-Q. Huang, and Q. Zhang, *Angew. Chem. Int. Ed.*, **57**, 14055 (2018).
7. H. Yang, X. Chen, N. Yao, N. Piao, Z. Wang, K. He, H. M. Cheng, and F. Li, *ACS Energy Lett.*, **6**, 1413 (2021).
8. Z. L. Brown, S. Heiskanen, and B. L. Lucht, *J. Electrochem. Soc.*, **166**, A2523 (2019).
9. J. Uddin, V. S. Bryantsev, V. Giordani, W. Walker, G. V. Chase, and D. Addison, *J. Phys. Chem. Lett.*, **4**, 3760 (2013).
10. V. Giordani, W. Walker, V. S. Bryantsev, J. Uddin, G. V. Chase, and D. Addison, *J. Electrochem. Soc.*, **160**, A1544 (2013).
11. W. Walker, V. Giordani, J. Uddin, V. S. Bryantsev, G. V. Chase, and D. Addison, *J. Am. Chem. Soc.*, **135**, 2076 (2013).
12. Y. Hayashi, S. Yamada, T. Ishikawa, Y. Takamuki, M. Sohmiya, H. Otsuka, K. Ito, Y. Kubo, and M. Saito, *J. Electrochem. Soc.*, **167**, 020542 (2020).
13. D. Sharon, D. Hirsberg, M. Afri, A. Garsuch, A. A. Frimer, and D. Aubach, *J. Phys. Chem. C*, **118**, 15207 (2014).
14. D. Sharon, D. Hirsberg, M. Afri, F. Chesneau, R. Lavi, A. A. Frimer, Y. K. Sun, and D. Aurbach, *ACS Appl. Mater. Interfaces*, **7**, 16590 (2015).
15. M. Saito, T. Fujinami, M. Sohmiya, Y. Hayashi, K. Koyama, H. Otsuka, K. Ito, Y. Kubo, and T. Horiba, *J. Electrochem. Soc.*, **168**, 010520 (2021).
16. L. Carbone, D. D. Lecce, M. Gobet, S. Munoz, M. Devany, S. Greenbaum, and J. Hassoun, *ACS Appl. Mater. Interfaces*, **9**, 17085 (2017).
17. M. Ue, H. Asahina, S. Matsuda, and K. Uosaki, *RSC Adv.*, **10**, 42971 (2020).
18. K. Edström, M. Herstedt, and D. P. Abraham, *J. Power Sources*, **153**, 380 (2006).
19. F. Shi, A. Pei, D. T. Boyle, J. Xie, X. Yu, X. Zhang, and Y. Cui, *Proc. Natl. Acad. Sci. U.S.A.*, **115**, 8529 (2018).
20. Y. Zhang, Y. Zhong, S. Liang, B. Wang, X. Chen, and H. Wang, *ACS Mater. Lett.*, **1**, 254 (2019).
21. L. Chen, A. Lv, F. Guo, M. Wang, and S. Jiao, *ACS Sustainable Chem. Eng.*, **8**, 706 (2020).
22. Y. Liang, W. Wu, D. Li, H. Wu, C. Gao, Z. Chen, L. Ci, and J. Zhang, *Adv. Energy Mater.*, **12**, 2202493 (2022).
23. X. Xin, K. Ito, A. Dutta, and Y. Kubo, *Angew. Chem., Int. Ed.*, **57**, 13206 (2018).